https://doi.org/10.5194/egusphere-2026-1564
Preprint. Discussion started: 9 April 2026

Biosignatures of microbial mats in Pleistocene coral reef cores from IODP Expedition 389 (Hawaiian Drowned Reefs)

Hildegard Westphal[1,2], Elisa Garuglieri[3], Gregory E. Webb[4], Luke Nothdurft[5], Anna Merkel[6], Pankaj Khanna[7], Poornima Karki[7], Theresa Nohl[8], Eberhard Gischler[9], Jody M. Webster[10]

[1]Leibniz Centre for Tropical Marine Research, Bremen, Germany
[2]Department of Geosciences, University of Bremen, Bremen, Germany
[3]Physical Science and Engineering Division, KAUST, Saudi Arabia
[4]School of the Environment, The University of Queensland, Brisbane, Qld 4072, Australia
[5]School of Earth and Atmospheric Sciences Faculty of Science, Queensland University of Technology, Brisbane, QLD, Australia
[6]GeoZentrum Nordbayern, Friedrich-Alexander-Universität Erlangen-Nürnberg, Germany
[7]Department of Earth Sciences, Indian Institute of Technology Gandhinagar, Department of Earth Sciences, Indian Institute of Technology Gandhinagar, India
[8]University of Vienna, Department of Palaeontology, Vienna, Austria
[9]Institut für Geowissenschaften, Goethe Universität, Frankfurt am Main, Germany
[10]Geocoastal Research Group, School of Geosciences, The University of Sydney, NSW 2006, Australia

Correspondence to: Hildegard Westphal (hildegard.westphal@leibniz-zmt.de)

Abstract. We systematically document surfaces and biosignatures of Pleistocene reefal microbialites (Marine Isotope Stages 7-6) recovered during IODP Expedition 389 (Hawai'ian Drowned Reefs). Microbialites are abundant within Pleistocene coral reef successions and offer valuable archives of environmental information under Quaternary climate variability. However, relatively little is known about biofilm-forming microbial consortia, because biosignature preservation is usually very poor. The microbial crusts studied here form encrustations as much as 20 cm thick, ranging from laminated to thrombolitic, within the coral reef framework. Scanning electron microscopy (SEM) of samples from the windward (humid) Hilo and Kohala and the leeward (arid) Kawaihae sides of the Island of Hawai'i reveals exceptionally well-preserved microbial fabrics that developed during Marine Isotope Stages (MIS) 7-6. Humid side samples exhibit abundant preserved putative exopolymeric substance (EPS) matrices, mineralized filaments, and near spherical, multilobate aggregates that resemble protodolomite spherules formed by modern cyanobacteria or extant coccoid cyanobacteria (e.g., Gloeocapsa-type). In either case, the surfaces appear to have been formed with significant aid of cyanobacteria suggesting formation in a euphotic setting. The microbialites from the arid side display peloidal microfabrics with fewer preserved physical biosignatures, typical of cryptic reefal microbialites, but the surfaces suggest confinement by an organic biofilm. The occurrence of pyrite framboids and huntite-like crystals in the wet-side samples suggests local redox gradients consistent with both sulphate reducing bacteria and cyanobacteria mediating carbonate precipitation. These findings provide the first direct evidence for euphotic microbial mat communities contributing to microbialite formation in Pleistocene drowned Hawai'ian reefs, and, to our knowledge, in

https://doi.org/10.5194/egusphere-2026-1564
Preprint. Discussion started: 9 April 2026

Indopacific reefs and beyond. The outstanding preservation of mineralized EPS and microbial morphotypes highlights the potential of these Pleistocene reefal microbialites as sensitive archives of palaeoenvironmental conditions and microbial diversity under glacio-eustatic forcing and associated environmental changes.

1 Introduction

Microbialites are organosedimentary deposits formed by benthic microbial communities through processes such as trapping, binding, and mineral precipitation, and represent some of the most ancient ecosystems in Earth's history and the first to form hard frameworks (Burne and Moore, 1987; Riding et al., 2000a). Their fossil record spans at least 3.5 billion years, providing insights into early life, biogeochemical cycling, and environmental conditions across geologic time (Grotzinger and Knoll, 1999; Riding et al., 2000b; Riding, 2006; Allwood et al., 2006). While marine stromatolites were globally dominant during the Precambrian and re-emerged prominently following mass extinction events (e.g., the end-Permian; Schubert and Bottjer, 1992; Baud et al., 1997; Webb, 2005; Pei et al., 2022), other microbialite types were important constituents of skeletal reefs throughout the Phanerozoic (e.g., Pratt, 1982; Webb, 1996). Microbialite occurrence in the Pleistocene in coral reef-associated, high-diversity, normal marine environments has drawn increasing attention for understanding carbonate platform dynamics and geomicrobiological processes under Quaternary climate variability (Reid et al., 2000; Dupraz and Visscher, 2005; Riding et al. 2014; Salas-Saavedra et al., 2022).

Pleistocene reefal microbialites provide archives of environmental change associated with glacio-eustatic and climatic fluctuations, since the microbial communities involved in their formation are highly sensitive to environmental parameters that affect metabolic processes and marine pH (cf. Riding, 2000b, 2014; Webb and Kamber, 2010). Specifically, Pleistocene reefal microbialites have been documented across a range of tropical and subtropical carbonate provinces, including the western Atlantic, Indo-Pacific, Arabian Gulf, and the Red Sea (Camoin et al., 1999; Reitner et al., 2000; Westphal et al., 2010; Heindel et al., 2012; Braga et al., 2019, among many others). Most, but not all, occurrences are linked to deglacial phases and transgressive reef systems and possibly lagoonal back-reef environments (White et al., 1984; Camoin et al. 1999; Szilagyi et al., 2020). Holocene microbialite crusts from Tahiti were interpreted early on as bio-accretionary features (Camoin and Montaggioni, 1994). In general, such microbialite formation requires: 1) a microbial consortium, 2) an organic carbon source (a local primary producer acting as energy source for microbial metabolism) that may, or may not, be a major part of the microbial community, 3) an appropriate nucleation template or scaffold to localize and support mineral precipitation (typically microbial exopolysaccharides - EPS), and 4) a local driver of increased pH and/or alkalinity, generally associated with microbial metabolism (Castanier et al. 1999; Visscher and Stolz, 2005; Dupraz et al., 2009; Heindel et al., 2010; Webb and Kamber, 2011). A general perception exists that the best-known microbialites, benthic stromatolites, are made by cyanobacteria. Although photosynthetic removal of CO_2 by cyanobacteria and filamentous green algae can increase pH within benthic biofilms, carbonate precipitation is also driven by processes deeper within the mat, where microbial heterotrophy processes organic matter from the overlying primary producers. Here, heterotrophs can modify potential nucleation scaffolds

https://doi.org/10.5194/egusphere-2026-1564
Preprint. Discussion started: 9 April 2026

(i.e., EPS) and create anoxic microenvironments where sulphate reduction, and other heterotrophic metabolic processes can deeply influence pH, increasing local alkalinity (Castanier et al. 1999; Dupraz et al., 2009; Heindel et al., 2010). The mechanisms involved in microbial carbonate formation within variably confined microenvironments (Dupraz et al., 2009; Webb and Kamber, 2011) are complex, ranging from rather passive mineralization of fresh or degraded EPS to mineral precipitation induced by microbial activities (organomineralization and biologically induced or influenced mineralization, respectively; e.g., Reitner et al., 1995; Garuglieri et al., 2024). In all cases, the higher the ambient $CaCO_3$ saturation state, the easier it is for microbial carbonate to accumulate (Riding and Liang, 2005), and microbialite mineral precipitation itself may occur only in highly chemically evolved microenvironments very different from the ambient one that surrounds them (e.g., anoxic versus fully oxygenated; Nothdurft et al., 2007). Hence, microbialites represent a combination of biotic and abiotic factors, thus providing a wealth of (paleo)environmentally significant morphological, textural, mineralogical and biogeochemical information (e.g., Riding, 2000b; Riding and Awramik, 2000; Dupraz and Strasser, 2002; Westphal et al., 2010; Webb and Kamber, 2010).

Reefal microbialites have a variety of morphologies and textures including laminated, thrombolitic, or dendritic structures formed mainly in aphotic (Reitner et al., 1995; Webb and Jell 1997) to euphotic (shaded?) shallow cryptic reef settings (Westphal et al. 2010), while benthic examples occur in deeper fore-reef slope settings (Heindel et al., 2010; Riding, 2011; Braga et al., 2019; Szilagyi et al., 2020). The study of Pleistocene microbialites from Tahiti (IODP Expedition 310) and the Great Barrier Reef (IODP Expedition 325) pointed to sulphate-reducing bacteria as the main drivers of carbonate precipitation in reefal microbialites (Heindel et al., 2009a; Braga et al., 2019). Nevertheless, the roles of differing trophic levels and metabolic pathways for microbialite formation in general have not been unraveled, and many potential variables exist (e.g., benthic versus tight cryptic, and euphotic versus aphotic settings). Of particular interest for the IODP Expedition 389 successions from leeward and windward settings is that microbialites are affected by differing or fluctuating terrigenous sediment and nutrient flux caused by differences in geography and changing climatic (cf. Reitner, 1993; Camoin et al., 1999) and oceanographic conditions (more intense circulation during deglaciation causing upwelling; cf. Marshall and Davies, 1988). Additionally, changing atmospheric pCO2 levels greatly affect marine carbonate saturation (Riding et al. 2014; Szilagyi et al., 2020).

A major hindrance to understanding microbialites is the fact that different indicators highlight different aspects of microbialite formation. While biomarker analyses in previous studies point to heterotrophic bacteria (i.e., light-independent organisms) steering calcification, microbioerosion patterns in the surfaces of microbialites (Heindel et al., 2009b) and the taxa of interlayered red algae (Westphal et al., 2010) are consistent with euphotic conditions where the primary producers could have been cyanobacteria. Other reef microbialites formed entirely in aphotic crypts (Webb and Jell, 1997; Gischler et al., 2017) where primary producers may have been cryptic sponges and ascidians (Reitner et al., 1995; Braga et al., 2019; Maak et al., 2024). This emphasizes the broad range of environmental requirements and mechanisms for growth of different reefal microbialites, but also highlights an enigmatic gap in the record of possible photoautotrophic bacteria in the microbialites that formed in euphotic conditions; their presence currently can only be hypothesized. The questions remain as to what are the

https://doi.org/10.5194/egusphere-2026-1564
Preprint. Discussion started: 9 April 2026

primary producers in reef microbialite consortia, and what types of communities or bulk metabolisms drive most mineral precipitation? Until we understand those issues, it will be difficult to retrieve all of the potential environmental data that microbialites record.

The preservation of identifiable microbial remains is generally poor in most microbialites except for calcimicrobes, which were common only in Paleozoic reefs (Webb 1996). In that case, carbonate precipitated on or replaced EPS, thereby preserving microfossils (e.g., the preserved filament sheaths of *Girvanella*; Zhang et al., 2024). However, precipitation may occur only on degraded organic matter and EPS deeper within the mat, thus preserving organic matter that lacks easily identifiable morphology (Reitner et al., 1995). Additionally, continued alkalinity generation beneath the confining active mat, may then drive additional precipitation, coarsening original crystals over time and further overprinting any original organic morphology (e.g., Webb et al., 1998). Thus, preservation of microfossils in microbialites is the exception to the rule (Webb and Kamber, 2010). However, where abundant precipitation occurs near the accretionary surface of the mat, recognizable and informative fossilized microbes may be more abundant.

Prior to the drilling of IODP Expedition 389, the reefal microbialites of Hawaii attracted little attention (Webster et al., 2009). Limited to ROV and dredge samples, two microbial fabrics were observed in samples from the top of Hawaiian drowned reefs: peloidal sediment filled cavities and laminated to clotted micrite crusts, as much as 5 cm thick, in some cases forming digitate stromatolite overgrowths. Both fabrics were interpreted to postdate the deep-water coralline-algal facies (60-120 m), indicating deposition at greater depths as part of the drowning sequence (Webster et al., 2009). High recovery and extremely good core quality of IODP Expedition 389 now allow for detailed study of the reef components and succession (Webster et al., 2025). Here we present the first results of a study of MIS 7-6 aged (approximately 133-225 kyr, Webster et al., 2025) reefal microbialites, shedding light on the architecture and microbial contribution to microbialites formation in coral reefs.

2 Study area and material

IODP Expedition 389 aimed to explore the drowned coral reefs on the rapidly subsiding margins of Hawai'i as archives of sea level and climate change (Webster et al., 2023). As a direct result of Hawai'i's rapid and nearly constant subsidence caused by flexure of the oceanic lithosphere (2.5–2.6 m/ky; Watts, 1978; Webster et al., 2009; Puga-Bernabéu et al., 2016), a 100–200 m thick expanded sequence of shallow coral reef-dominated facies is preserved within the terraces off the Hawai'ian coast. Thus, Hawai'ian reefs cover the time intervals leading into, during, and out of the majority of the last five to six glacial cycles (Webster et al., 2023, 2024, 2025). One objective of this expedition was to gain a better understanding of ancient microbial communities within the reefs and their role in reef building. Based on compiled bathymetric data sets, 13 major terraces were identified around the Island of Hawai'i (designated H0–H12 from shallowest to deepest, where "H" is for Hawai'i) (Webster et al., 2009; Puga-Bernabéu et al., 2016; Sanborn et al., 2017; Taylor 2019). Drilling operations took place from September to November 2023 with a seafloor drill (PROD5), achieving very good recovery (Webster et al., 2024). Besides well-preserved corals, the cores contain a high percentage of microbialites in the coral reef succession, forming crusts up to 20 cm in thickness

https://doi.org/10.5194/egusphere-2026-1564
Preprint. Discussion started: 9 April 2026

and making up a substantial portion of the recovered lithologies (Webster et al., 2025). Here we study the H2 terrace as recovered at Sites M0097, M0102, and M0104 (Fig. 1). The H2 terrace, with the top dated at 130 kyr, developed primarily during MIS 7-6, before drowning during the transition to MIS 5e (Fig. 2).

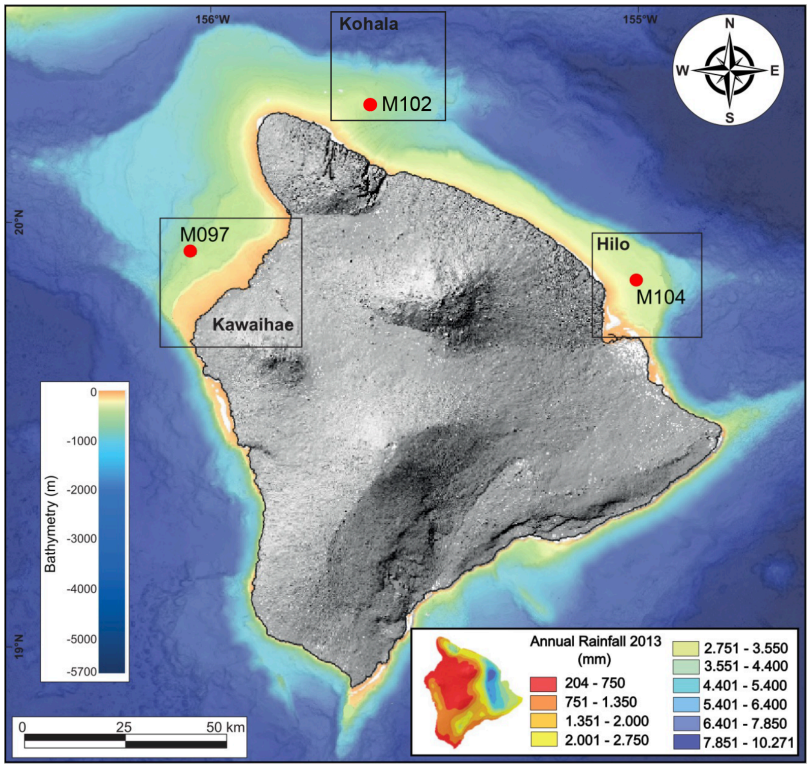

Figure 1: (A) IODP Expedition 389 drill sites M0097, M0102, M0104 studied here; bathymetric map from SOEST (2016; see Webster et al., 2024). Map of modern precipitation in the inset (Sanfilippo et al., 2024).

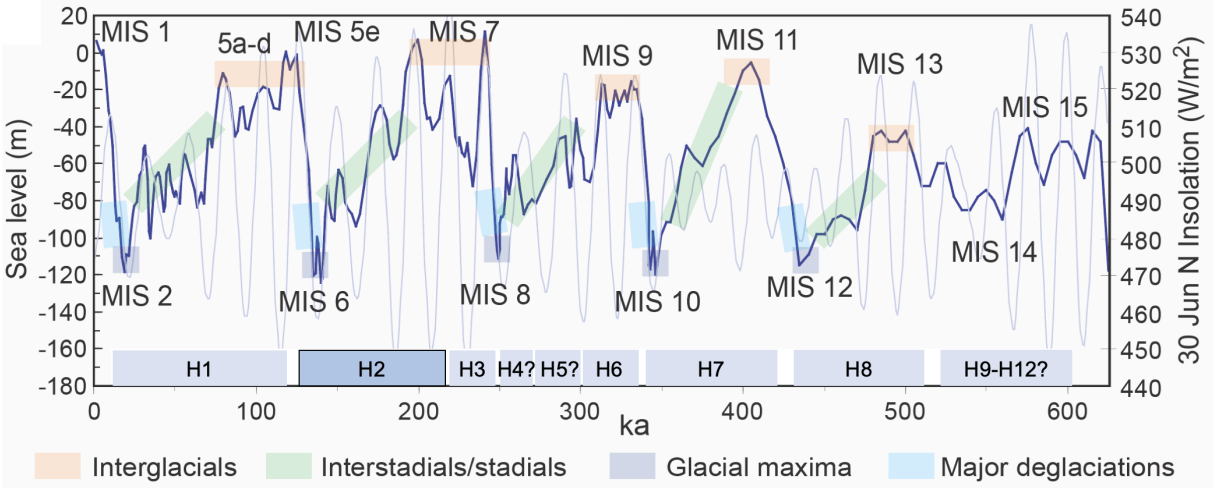

https://doi.org/10.5194/egusphere-2026-1564
Preprint. Discussion started: 9 April 2026

Figure 2: Sea level, insolation and reef terraces around the Island of Hawai'i over the last 600 ky (after Imbrie et al., 1984; Berger and Loutre, 1991; Lea et al., 2002). Observational and numerical modeling data indicate that the Hawaiian reef successions (H1–H12) span each interglacial, interstadial/stadial, glacial maxima, and deglacial interval over the past 500-600,000 years with only minor hiatuses (Webster et al., 2009). The present study focuses on the H2 terrace.

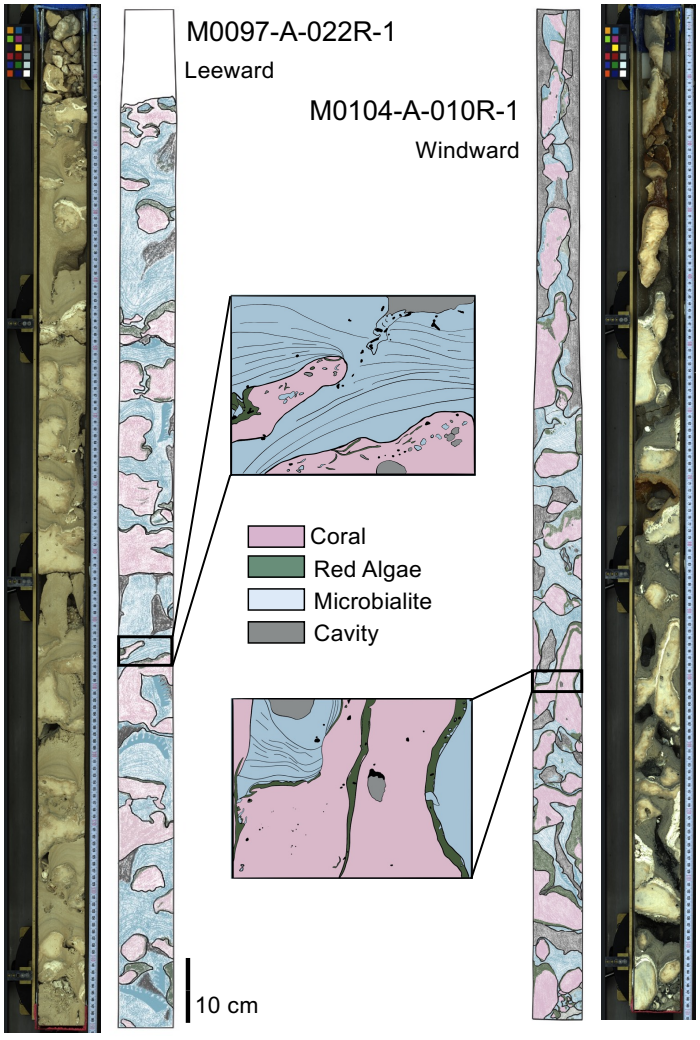

Figure 3: Examples of core section line scans from the arid (M0097) and humid side (M0104) of the island of Hawaii, along with the interpretation of coral, encrusting red algae, and microbialite contribution to the reef framework. The close-ups illustrate the occurrence of laminated microbialites.

The reefal microbialites in the Hawai'ian succession typically occur as the latest stage of framework sequence, overgrowing the coralgal framework and partly filling cavities in the reef or under ledges created by platy corals (Fig. 3). They form laminated and thrombolitic textures, in most cases occurring on top of red algae crusts had previously encrusted corals (Webster

https://doi.org/10.5194/egusphere-2026-1564
Preprint. Discussion started: 9 April 2026

et al., 2025). This is similar to previously described successions from other locations, such as Tahiti (e.g., Westphal et al., 2010) and the Great Barrier Reef (Braga et al., 2019), where microbialites were interpreted to develop coevally to, or immediately after coral growth, while the reef is still in the photic zone (Heindel et al., 2009b; Westphal et al., 2010; Jell and Webb, 2012). Although representing the latest stage of encrustation, these decimeters-thick microbialites do not completely fill the macropore space of the reef framework. In Tahiti the microbial crusts were estimated to account for as much as 80% of reef rock volume (Séard et al., 2011) and ~43-72% in the IODP 325 cores from the GBR (Szilagyi et al., 2020). As in the Tahitian microbialites, there is a distinct difference in coloration related to humidity and run-off patterns in the Hawai'ian microbialites, with the arid side of the island featuring lighter colors as compared to the humid side (Fig. 2; Webster et al., 2025).

In this study, we compared H2 terrace (MIS7 to MIS6; Webster et al., 2025) microbialites from the windward, humid side of the island (Sites M0102 and M0104) with those from the leeward, dry side (Site M0097) (Fig. 1; Fig. 3; Appendix A) specifically to identify any morphological biosignatures and document possible differences in microbial signatures between the two settings. A total of seven samples were chosen that have clear, undamaged accretionary surfaces where microbialites grew into reef framework voids, i.e., the final stage of growth (Fig. 4; Appendix B). For identifying the microbialites, we followed the criteria of Webb and Kamber (2010), namely the macro-morphology, the micro-morphology, and the appropriate environment (see: Webster et al., 2025), with a special focus on the fourth criterion, i.e., the preservation of morphological bioindicators of microbes as part of the texture.

https://doi.org/10.5194/egusphere-2026-1564
Preprint. Discussion started: 9 April 2026

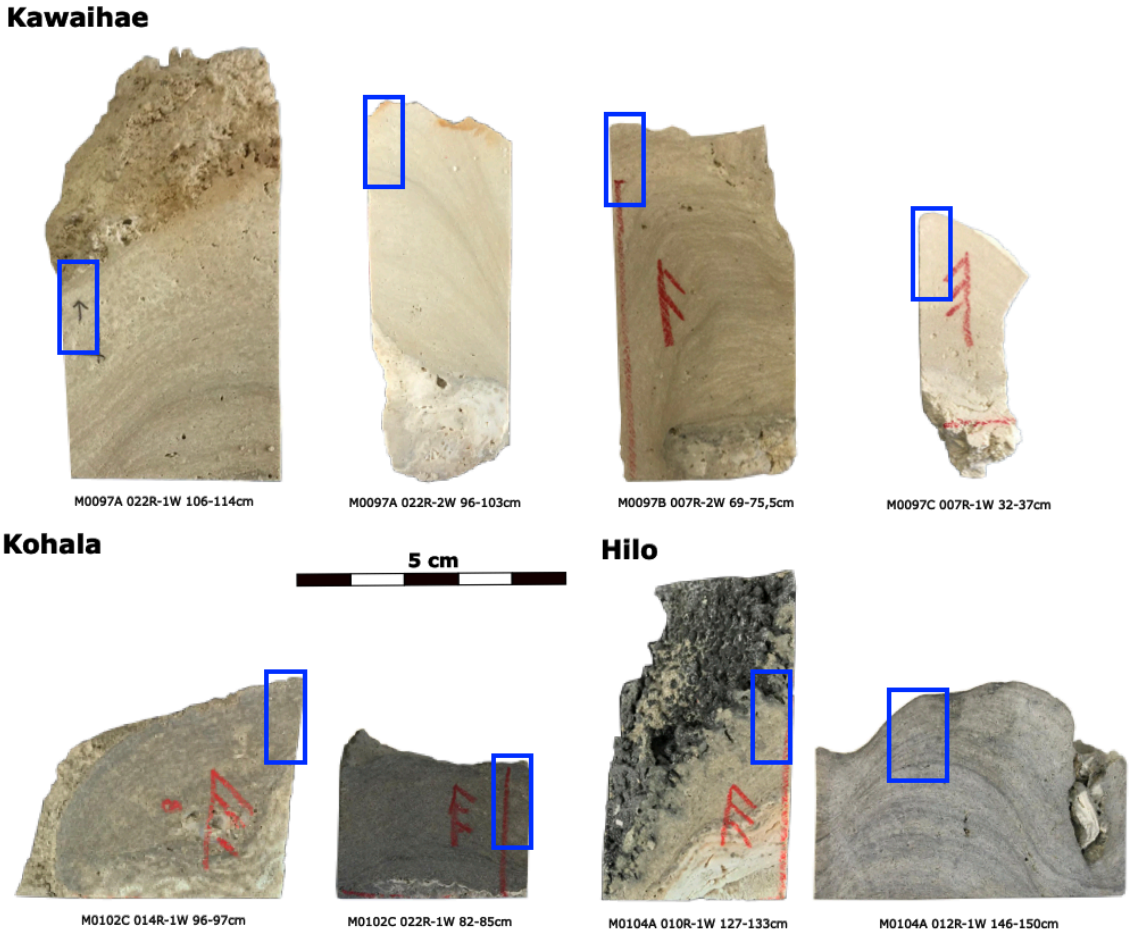

Figure 4: Samples studied by SEM; blue quadrangles indicate the two subsamples prepared for SEM microscopy.

3 Methods

Samples were examined under a scanning electron microscope (SEM) to identify the remains of microbes that allow for biological identification. With SEM imaging of microbialite surfaces and vertical polished sections, we characterize the ultrastructure of the crusts and identify trapped and bound particles (e.g., *Cliona* sponge chips from bored reef skeleton; de Bakker et al., 2024) as well as any microbial remains that might allow identification of the microbes, e.g., filaments that are indicative of taxonomic determination (cf., Melim et al., 2015).

Prior to analysis, the outermost growth surfaces of microbialites facing voids in the reef edifice were identified. These surfaces were sampled and mounted on SEM stubs. From the same samples, subsamples were cut perpendicular to the laminations and polished with corundum powder (borcarbid 400 and 600). All samples were then cleaned in an ultrasonic bath and rinsed with

https://doi.org/10.5194/egusphere-2026-1564
Preprint. Discussion started: 9 April 2026

Millipore water, although in some cases salts were not entirely removed. Cut samples were then etched with 0.3% (0.1 N) hydrochloric acid for 20 seconds. Note that the preparation including ultrasonic cleaning as well as the etching of the cut surfaces prevents contamination. All samples were dried and coated with iridium (10 nm). SEM analysis with a secondary electron (SE) detector was performed with a Teneo-VS SEM at the KAUST Imaging and Characterization Core Lab, and a Tescan Vega LMU at the ZMT Geosciences Laboratory. Element concentrations were measured with an Oxford Energy Dispersive X-ray (EDX X-Max SDD; detector: 50 mm^2) coupled to the Tescan Vega LMU. EDX working parameters were set to a beam voltage of 10 kV, a maximum of 5 million counts with a peak pile-up correction, and a process time of 4 min. Dead time was set to 30–50%.

X-ray diffraction (XRD) pattern analyses were conducted in the laboratories of the Crystallography and Geomaterials Research Group at the Department of Geosciences, University of Bremen. Dried bulk samples were ground to a fine powder (<20 µm particle size) and prepared with a Philips backloading system. For XRD analysis, a Bruker D8 Discover diffractometer was used. The instrument was equipped with a Cu-tube (k_α 1.541 Å, 40 kV, 40 mA), and a fixed divergence slit of ¼°, a monochromatization via energy discrimination on the highest resolution Linxeye detector system. Measurements were taken as a continuous scan from 3 – 65° 2θ, with a calculated step size of 0.016° 2θ. Mineral identification was done with the Philips software X'Pert HighScore™ Vs. 1.2 (Degen et al., 2014). The determination of well crystallized minerals like quartz, calcite or aragonite has a standard deviation of ± 1-3 % (Hardy and Tucker, 1988, Vogt et al., 2002).

4 Results

4.1 Hilo and Kohala sites - Humid, windward margin

The microbialites from the humid side of Hawai'i are organized in layers, five of which can be distinguished on the basis of textures and biomorphic structures (Fig. 5).

Layer 1: The surfaces of the microbialites are smooth, consisting of fine, poorly oriented anhedral crystals. This smooth layer with a thickness on the order of max. 1 mm consistently makes up the uppermost element of the microbialite (Fig. 5A-C, G). At high magnification, the outer layer locally appears to be composed of irregular material with abundant molds in a matrix showing curved surfaces consistent with mineralized EPS or mucilage residues (Fig. 6C, D, J). Very smooth, cracked surfaces could represent a modern biofilm that has colonized the older microbialite surface (Fig. 6B). The samples contain abundant trapped and bound skeletal grains as well as non-carbonate detritus (Fig. 6B, H), the latter showing an elemental composition pointing to silicates (Appendix C). Cross section samples from the windward, humid, side of the island (Fig. 6H-N) show some layering and diffuse porosity (Fig. 6A) with interconnected voids (Fig. 6E).

https://doi.org/10.5194/egusphere-2026-1564
Preprint. Discussion started: 9 April 2026

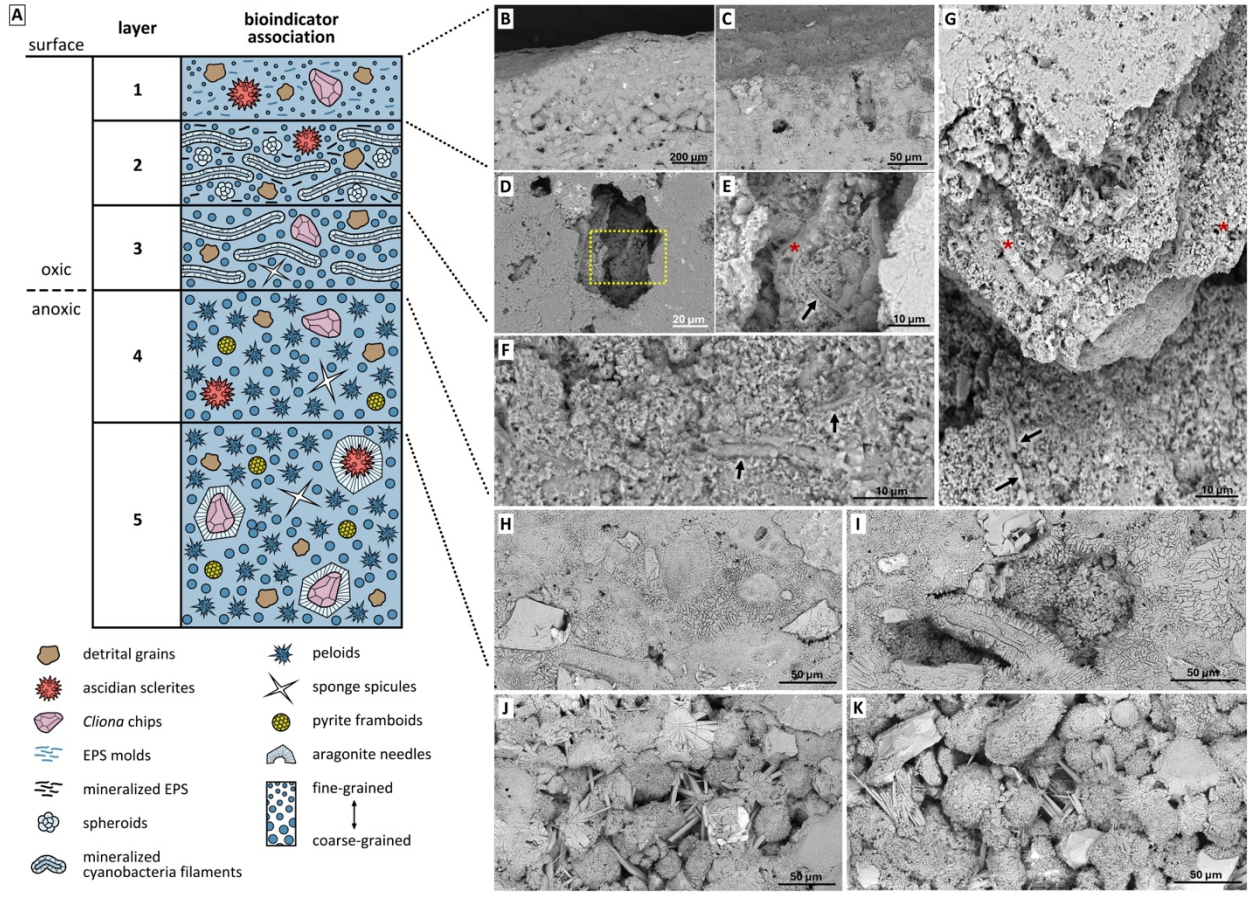

Figure 5: Typical textures of layers composing microbialites on the humid side of the Island of Hawai'i. (A) Schematic of the five observed layers; (B, C) cut through the surface of the microbialite (Layer 1) showing fine crystalline texture and trapped grains; (D) collapsed surface layer revealing underlying Layer 2; (E) enlargement of Layer 2 showing filamentous biomorphs; (F) Layer 3 with altered and tightly cemented biomorphs; (G) view of Layers 1, 2, and 3 in a broken surface of a microbialite; (H, I) increase in crystal size of cements enclosing trapped and bound grains with cement showing peloidal textures in Layer 4; (J, K) peloidal texture and syntaxial aragonite needle cement on ascidian spicules in Layer 5 samples.

https://doi.org/10.5194/egusphere-2026-1564
Preprint. Discussion started: 9 April 2026

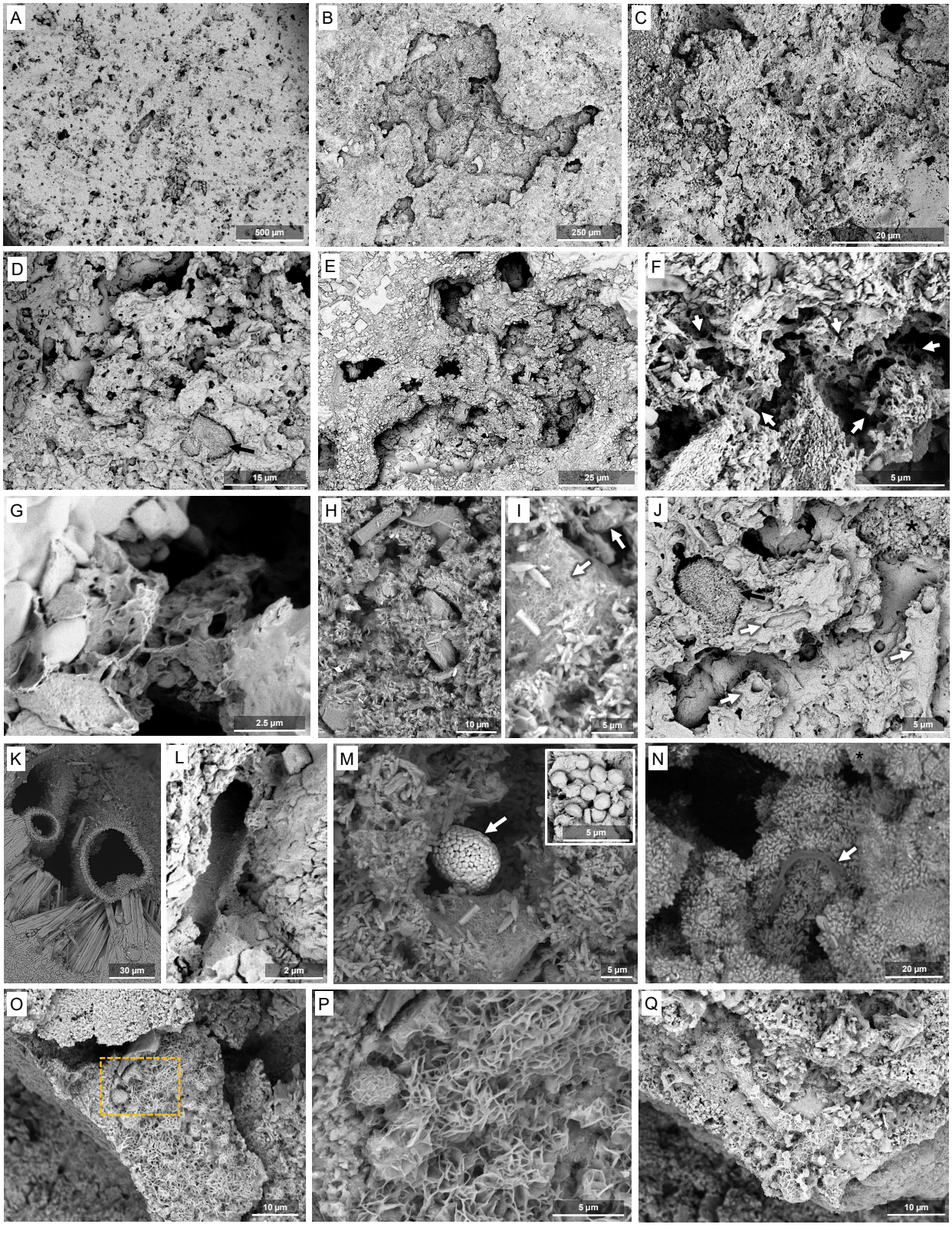

https://doi.org/10.5194/egusphere-2026-1564
Preprint. Discussion started: 9 April 2026

Figure 6: SEM images of samples from the humid side of the Island of Hawai'i. Layer 1: (A-E, J-N); Layer 2: (F,G, O-Q). (A) Low magnification image of cross-section of the fine-crystalline surface. (B) Surface sample showing a collapsed area on the sample surface revealing underlying Layer 2. (C, D) Higher magnification of the fine-crystalline surface layer material consistent with torn, desiccated, and mineralized EPS. (E) Porous spaces coated by microcrystals. (F, G) Details of torn, laminated matrix-like material consistent with fossilized EPS residues (white arrows). (H) Acicular microcrystals. (I) Microcrystals associated with bladed minerals (white arrows). (J) Mineralized filamentous structures preserved as hollow tubes (white arrows). (K) Calcified anastomosed tubes coated with crystals of various dimensions. (L) Hollow calcified sheaths of filamentous bacteria. (M) Pyrite aggregates. (N) Microbial filaments located within a porous space (white arrow). (O) Flaky precipitates covering spherical biomorphs, (P) close-up of (O). (P) Flaky precipitates covering filamentous biomorphs. (H, I, K, M): Site M0102C, core section 22, all others: Site M0104A, core section 12.

Layer 2: Beneath the outer smooth, fine-crystalline Layer 1, mineralized biofilms with preserved filaments occur (Layer 2, Fig. 5A, C, E, G). A remarkably well-preserved microbial mat shows mineralized remains of EPS, isolated and aggregated filaments and a variety of spheroids (Fig. 7). Microbial bioindicators are abundant, including spheroidal and filamentous morphotypes (Fig. 7A-I; black and white arrows, respectively) embedded within the smooth, drape-like matrix. The filamentous morphotypes are horizontally oriented. Globular spheroids of variable size and morphology (Fig. 7B-F; white arrows) are consistently arranged in clustered aggregates. Smaller coccoid forms are also present (Fig. 7D, F). Filamentous structures exhibit a relatively uniform diameter (2–3 µm) and are predominantly preserved as hollow, mineralized sheaths (Fig. 7C, D, G-I, black arrows). Further preserved biological structures at the surface of the mineralized biofilms include mineralized EPS, hollow tubes and filaments (Fig. 6C, D, F, J, N). Filament-rich matrix-like materials similar to those encountered on the surface also occur (Fig. 6F, white arrows, and 6G). Irregular needle-fiber crystal aggregates are consistent with thin fossilized EPS residues, possibly at a more degraded stage compared to their surface counterparts (cf., Lin et al., 2019). The voids also contain anastomosed tubes (Fig. GK), hollow calcified sheaths of filamentous bacteria (Fig. 6L) and other microbial filaments (Fig. 6N). Locally, the tubes and spheroidal morphotypes show an overgrowth with flaky minerals (Fig. 6O-Q) with an elemental composition of Ca, Mg, Al, Si (Appendix D).

https://doi.org/10.5194/egusphere-2026-1564
Preprint. Discussion started: 9 April 2026

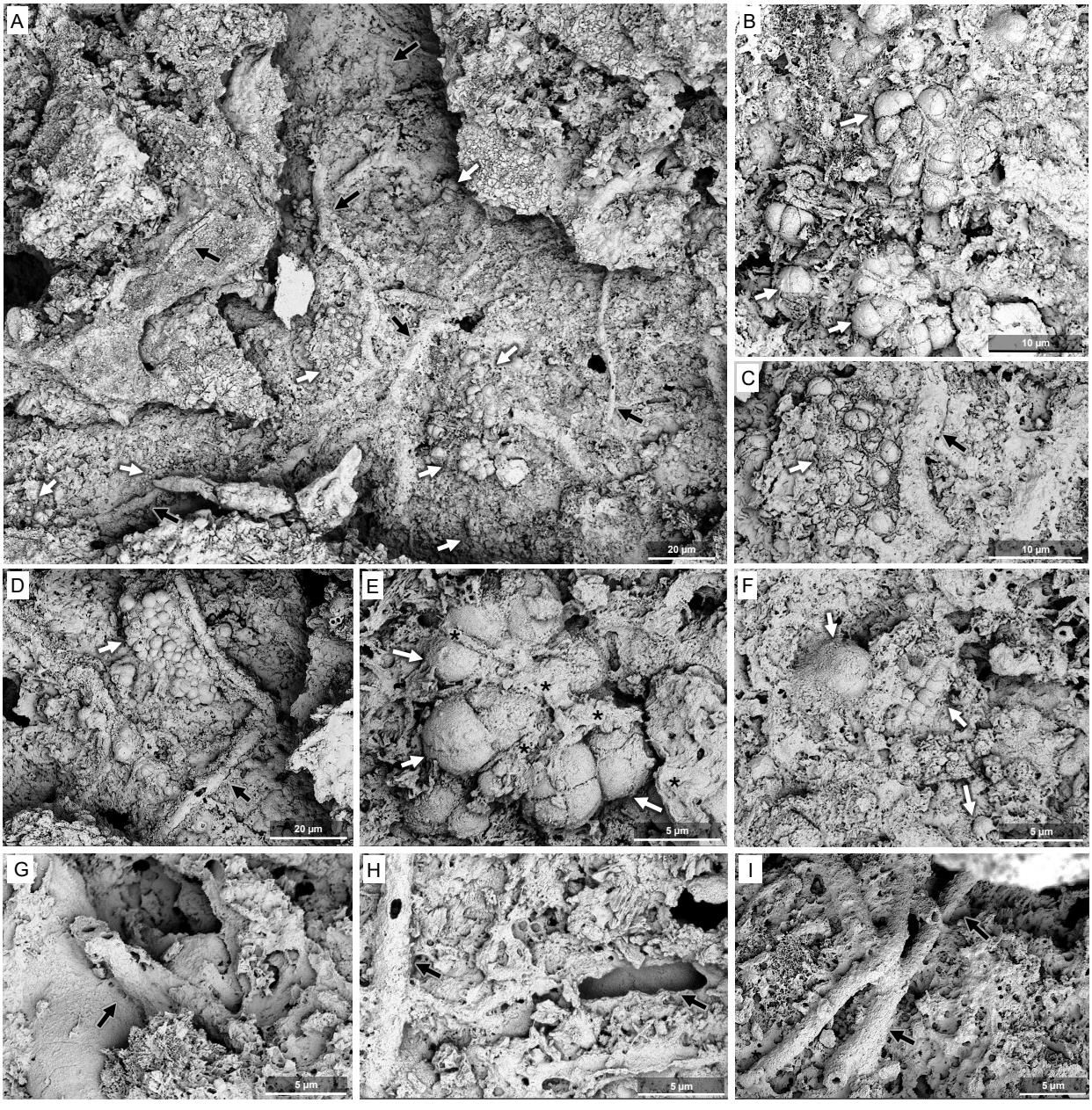

Figure 7: SEM images of the microbial biofilm (Layer 2) observed on the surface sample from the humid side of the Island of Hawai'i. (A) General view of the crack within the surface layer exposing the biofilm; white arrows indicate coccid biomorphs and black arrows filamentous biomorphs. (B) Details of a group of coccoid biomorphs (white arrows) emerging from copious EPS matrix. (C, D) Details of a group of coccoid structures (white arrow) showing mineralized EPS septa and a filamentous biomorph (black arrow) in two different locations of the biofilm area. (E) Details of a group of quadrilobed biomorphs (white arrows), similar to the modern genus *Gleocapsa*, surrounded by EPS sheaths (black asterisks). (F) Details of a group of coccoid biomorphs (white arrows) in a different spot of the biofilm area. (G-I) Mineralized hollow structures compatible with calcified sheaths of filamentous bacteria (black arrows). All images from Site M0104A, core section 12.

https://doi.org/10.5194/egusphere-2026-1564
Preprint. Discussion started: 9 April 2026

Layer 3: Further below that layer, microbial bioindicators such as filaments appear more altered, mineralized and tightly cemented in the matrix (Fig. 5A, F, G).

Layer 4: A downward coarsening of the cement crystals is observed in cross section Millimeters below the fine-crystalline surface layer, coarser crystals appear as well as peloidal textures (Fig. 5A, H, I, 6B, C, D). Peloidal textures are generally restricted to Layer 4 and below. The matrix encases rare nanocrystal aggregates (average aggregate dimension of 10 μm; Fig. 6D, J, black arrows), as well as diffuse microcrystalline areas with irregularly oriented crystals forming peloids or aggregates (Fig. 6H-J, M) and containing trapped and bound detritus, including arcuate chips of coral skeleton typical for the boring activity of the sponge *Cliona*, abundant ascidian spicules (Fig. 5H) and some calcareous sponge spicules. Pore are typically lined by more euhedral microcrystals (Fig. 6E, K, L, N). Fine-grained meshes of acicular microcrystals (Fig. 6H, I, M) and bladed minerals (Fig. 6I, white arrows) also occur. Pyrite framboids are present in Layer 4 (Fig. 6M).

Layer 5: While otherwise showing the same textural characteristics as Layer 4, in Layer 5, aragonite needle cements are present as syntaxial overgrowth on aragonitic skeletal grains such as ascidian spicules and coral skeleton cut in chips by the boring sponge *Cliona* (Fig. 5A, J, K).

4.2 Interpretation of Hilo and Kohala sites - Humid, windward margin microbialites

The smooth undulating surface crusts (Layer 1) and increasing euhedral crystal growth as well as intergrown peloids with depth (downwards towards Layer 4, Fig. 5) are consistent with patterns observed in Holocene-modern microbialite growth (Webb et al., 1998). However, the well preserved filaments and spheroids in Layer 2 with smooth, draping textures suggest abundant precipitation within the surface community where EPS and microbial sheaths were replaced by $CaCO_3$ (Webb and Kamber, 2010, their figure 2). The large filament diameter and prostrate growth is consistent with cyanobacteria. The spheroids are more difficult to interpret. Some quadrilobed forms (Fig. 7B, E) closely resemble those observed in extant cyanobacteria of the order *Chroococcales* (e.g., the genus *Gleocapsa*, of similar dimensions). However, similar features have been produced in cyanobacterial biofilms as protodolomite spheroids even mimicking a similar lobate morphology (e.g., Zhao et al., 2024). The great difference in diameter of some of the spheroids in some clusters observed in Layer 2 (Fig. 7D) is more consistent with mineral spheroids, but other clusters are more uniform (Fig. 7B, C, E). The mode of preservation may also favour mineral spheroids, as the filaments are preserved as mineralised sheaths left hollow by degradation of the cells within, whereas the spheroids do not appear to be hollow, so would presumaly represent perservation of the cells themselves. The large difference in diameter of spheroids between different clusters (Fig. 7A) suggests more than one process was operating in any case. Other holes in the EPS are consident with microbe moulds. Regardless, both spheroid interpretations suggest the presence of cyanobacteria, so we suggest that the microbialites formed in open crypts with abundant light and adequate nutrients to support a cyanobacterial community as the primary producer of organic matter. Trapped and bound material still include evidence of abundant cryptic reef dwellers (sponges and ascidians), but abundant coccoliths also occur consistent with nutrient-rich water.

https://doi.org/10.5194/egusphere-2026-1564
Preprint. Discussion started: 9 April 2026

While precipitation occurred in the top layers within the microbial mat (Layers 1-3), thus preserving the filaments of cyanobacteria (oxygenic photoautotrophs), additional precipitation occurred deeper within the mat (Layer 4) where degraded EPS was preserved and heterotrophs continued to produce alkalinity, coarsening microbial peloids and lining cavities with scalenohedra, through the activity of an anoxic community. The flaky precipitates with a silicate composition (Appendix D) observed on biomorphs (6 O-Q) could represent microbial autochthonous clay minerals. Preservation of pyrite framboids in deeper parts of the microbialite, for example, suggests ongoing sulphate reduction, but other processes, such as ammonification, also could have been important. The occurrence of syntaxial aragonite needle cements on skeletal grains suggests (Layer 5) a highly increased alkalinity allowing for precipitation below the main activity of sulphate reducing bacteria.

4.3 Kawaihae site – Arid, leeward margin

The samples from the dry side of the island lack the distinctive layers observed on the wet side. While no fossilized microbial mats were observed here, other indicators of microbial activity are abundant. Both, the growth surfaces (Fig. 8C, D) and the vertically cut samples (Fig. 8A, B, E, F) show massive and peloidal textures composed of variably sized and typically irregularly oriented microcrystals. Peloidal structures as shown in Figure 8D could have formed late in the microbialite formation owing to **endolithic activity in the pore spaces under the rock surface (cf., Falkenberg et al., 2026)**. The bulk surface appears to be composed of irregularly overlapping laminae that are relatively smooth and undulose in places and more irregular with abundant trapped and bound sediment in others (Fig. 8C). Micropeloidal textures and confining structures are consistent with a biological origin (Fig. 8D-F) and occur in all samples coalescing to form the mineral matrix with minor trapped and bound detritus including both cryptic calcareous sponge spicules and possibly coccoliths (Fig. 8C). Much of the surface consists of irregular peloidal fabric composed of variably sized, mostly irregularly oriented crystals ranging from finer anhedral to coarser subhedral-euhedral shapes. Rare hollow, spherical structures coated in crystals (Fig. 8C; orange square) and tubular filamentous biomorphs (Fig. 8F) also occur, compatible with calcified bacterial cells and strings. One nannolith with flowery appearance (Fig. 8C; yellow square) could represent a coccolith.

https://doi.org/10.5194/egusphere-2026-1564
Preprint. Discussion started: 9 April 2026

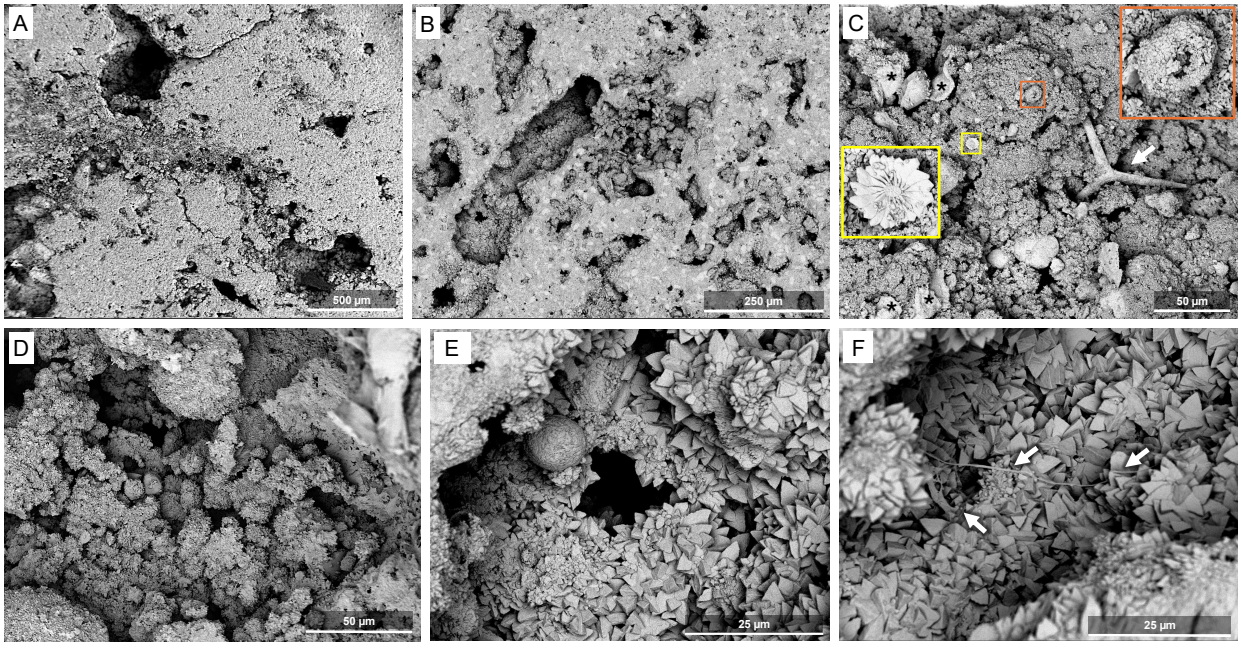

Figure 8: SEM images of samples from the Kawaihae site, i.e., the dry side of the Island of Hawai'i. (A, B) Low magnification micrographs of the vertically cut sample. (C) Assemblage of structures of possible biological origin found on the surface of the sample; torn sheet-like matrices compatible with desiccated EPS (black asterisks), a spherical hollow structure consistent with a lithified coccoid microorganism (orange square), a calcareous sponge spicule (white arrow) and a coccolith flowery plate possibly affiliated to Discoasteraceae (yellow square). (D) Peloidal texture with abundant spheroidal structures coated in fine crystals. (E) Cavity exposed by the cut, covered in a microcrystalline coat. (F) Filaments consistent with EPS strings, indicated by white arrows (F). All images from Site M0097B, core section 72.

Vertically cut samples are massive with porous zones serving to demarcate minor layering. Most of the micritic structure is composed of merged peloidal texture similar to that on the surface (Fig. 8A, B, E). Trapped and bound detritus is relatively rare but includes calcareous sponge spicules and chips excavated by the boring sponge *Cliona* from the skeleton of corals. The inner surfaces of voids are lined by coarser, more euhedral crystals (Fig. 8B, E, F) as already described in the surface samples. Biological structures and signatures are scarce here, consisting of spare microfilaments consistent with EPS fine strings (Fig. 8F). The presence of some characteristic smooth covers, in particular on the dry side of the islands, in both surface samples and cuts, may represent halite or organic matter remobilized during preparation.

4.4 Interpretation of Kawaihae site – Dry, leeward margin microbialites

The smooth undulating surfaces are consistent with formation at the base of a biofilm and is similar to other described reefal microbialites (Webb et al., 1998). The abundant peloids in deeper parts of the microbialites (millimeters depth) are typical of peloidal carbonates long associated with bacterial precipitation (e.g., Chafetz and Buczynski, 1992) and the coarsening of crystal texture below the surface is consistent with previous observations in reefal microbialites (Webb et al., 1998). The abundant holes or niches may have been colonized by endolithic microbial colonies, later covered of fine crystals coatings (cf.,

https://doi.org/10.5194/egusphere-2026-1564
Preprint. Discussion started: 9 April 2026

Falkenberg et al., 2026). The irregular fine-grained matrix is in places consistent with mineralized EPS (Dohlkanova et al., 2011). Trapped and bound material from boring and other cryptic sponges and the morphology described above is consistent with microbialite formation in semi-enclosed crypts within the reef framework with no obvious evidence of cyanobacteria.

4.5 Mineralogy

The microbialites from both sides consist mainly of high-Magnesium calcite (HMC) making as much as 89% of the samples (Appendix E). Aragonite amounts to as much as 15%, while anorthite, i.e., Ca-rich plagioclase, is present (as much as 7%) in samples from the windward side. Traces of quartz, huntite, and other minerals also were observed, but pyrite was not detected, despite framboidal pyrite being found in SEM analysis.

5 Discussion and Conclusions

The genesis of reefal microbialites is still poorly understood. While the involvement of cyanobacteria in the formation of microbialites has been discussed for more than a century (e.g., Holtedahl, 1919), it became clear that complex consortia forming microbial mats and creating a succession of microbial activity are involved (e.g. Stolz et al., 2009). As Webb (2005) pointed out, microbialites are not necessarily the product of certain taxa but rather of a diverse consortium of autotrophic and heterotrophic microbes. Nevertheless, previous studies of Pleistocene reefal microbialites remained inconclusive regarding the presence of cyanobacteria (e.g., Heindel et al., 2009a).

The Expedition 389 samples studied here resemble those presented in earlier studies (Heindel et al., 2010; Riding, 2011; Braga et al., 2019; Szilagyi et al., 2020) in their texture observed in deeper parts of the reef microbialite, including the abundance of *Cliona* chips, originating from coral skeletons, as reflected, together with some cements, in the aragonite portion reaching 15% of the bulk microbialite. However, in contrast to reefal microbialites studied earlier, the Hawai'ian microbialites exhibit an extraordinary preservation of microbial mats featuring cyanobacterial bioindicators. In particular, the samples from the humid side of the Island of Hawai'i show rich bioindicative features. The abundant occurrence of desiccated, cracked and mineralized EPS or mucilage residues in surface samples indicates that they indeed are ancient features, and have a distinctly different appearance than occasional spots of younger organic material accumulated during preparation on surfaces and cuts. This is also confirmed by the presence of degraded EPS signatures within the rock as exposed in vertical cuts of the samples.

Microbialite samples from IODP 389 reveals a succession of textures and bioindicators allowing for reconstruction of the successive microbial activities in the succeeding layers (Fig. 5). Figure 7 shows a microbialite surface from the humid side that exhibits a specifically copious and well-preserved layer of EPS. The mineralized EPS and biofilm show a "cracked" appearance of the uppermost layer of the surface specimen which, at closer look, is made of torn EPS matrix embedding hollow filamentous sheaths. In the same specimens, pyrite aggregates indicate a reducing micromilieu caused by heterotrophic oxygen removal that allowed sulphate reduction within the microbial mats and local redox gradients. This is consistent with the findings of Gomes et al. (2021) who showed microbial communities are likely to play a major role in promoting pyrite

https://doi.org/10.5194/egusphere-2026-1564
Preprint. Discussion started: 9 April 2026

formation at the surface of microbial mats. The origin of trace quartz identified in XRD measurements of samples from the windward side of the island is inconclusive. It may be autochthonous, representing remineralized diatom and siliceous sponge skeletons, or may be allochthonous sourced from Asian eolian dust as identified previously on Hawai'i (Kurtz et al., 2001). Quartz was not observed directly in SEM, so its morphology remains unknown.

The observed biofilm areas (Fig. 5-7) are particularly well-preserved, and allow characterization of a succession from fine-crystalline, smooth surface layers to "deeper" layers of the biofilm, followed by even deeper and more crystallized layers. Filaments that extend into the embedding EPS and sediments exclude that they are modern contaminants. The putative coccoid colonies are also completely embedded in the matrix, which shows the typical appearance of dehydrated EPS with calcified septa in some cell clusters. These spectacular microbial mats with diverse cell types (no bacilli, only globular/cocci and filamentous) and colonies support the hypothesis of an actual microbial multispecies biofilm or microbial mat, some of them consistent with cyanobacteria indicating that the microbialite originated in the photic zone.

In the samples from the dry side of the Island of Hawai'i, discrete layers of biomats were not identified, but similar biosignatures are present, albeit are less abundant as compared to the wet side. Also, fewer spicules of ascidians are identified. Encrusting ascidians are common inhabitants of reef cavities as shown for Lizard Island in the GBR, with their spicules being incorporated in microbialites (Reitner, 1993). As ascidians thrive in moderate to elevated nutrient levels (e.g., Ribes et al., 2005; Eckhard et al., 2024), thus a lower abundance on the humid side of the island might be expected.

The flaky and mesh-like minerals observed (Fig. 6O-Q) resemble the magnesium carbonate huntite known from microbialites forming in high-salinity/alkalinity crater lakes (Caumartin et al., 2025), or the magnesium carbonate dypingite that is known to be associated with modern cyanobacteria in alkaline wetlands (Power et al., 2007; Shirokova et al., 2013). It is known that EPS secreted by cyanobacteria can bind Mg^{2+}, creating microenvironments conducive to mineral nucleation (Robles-Fernández et al., 2022). Dypingite, however, does not form in marine waters and was never confirmed for reefal microbialites. Also, Mg clays can have a similar appearance and are known to form in the context of cyanobacteria (Perri et al., 2017). Therefore, an interpretation remains speculative. However, XRD analyses indicate the presence of traces of huntite, which is known to form in microbialites (Caumartin et al., 2025). The observation that high-Mg-calcite is so ubiquitous in reefal microbialites in general (Reitner, 1993; Camoin et al., 1999; Gischler et al., 2017) and in the Hawai'ian examples studied here in particular lends evidence to the presence of heterotrophic bacteria as well. Sulfate-reducing bacteria apparently exert control on calcium carbonate polymorph mineralogy in that high-magnesium calcite and dolomite precipitation occurred preferentially both in experiments and in a modern coastal lagoon environment (van Lith et al., 2003).

https://doi.org/10.5194/egusphere-2026-1564
Preprint. Discussion started: 9 April 2026

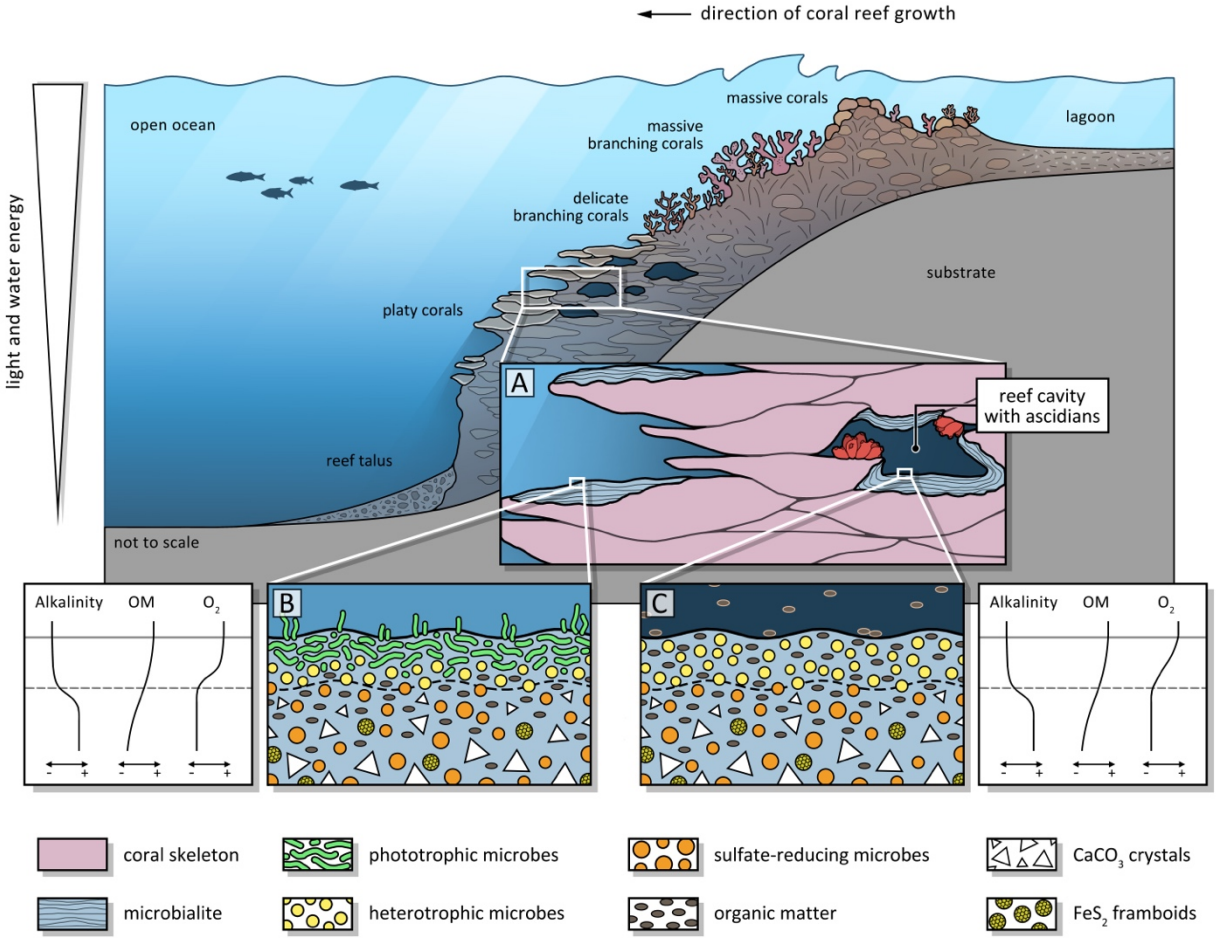

Figure 9: Schematic diagram of loci of microbialite formation in a coral reef under slightly shaded euphotic versus oligophotic cryptic conditions. Section through a coral reef, (A) euphotic versus cryptic setting in a cavity, (B) close-up of euphotic setting with cyanobacterial mat at the surface of the microbialite, (C) close-up of detrital organic matter-driven microbial mat in a cavity. Diagrams illustrating gradients in alkalinity, organic matter, and oxygen throughout the upper layers of the microbial mats.

Evidence found in the MIS 7-6 microbialite samples from the wet-side from IODP 389 allows us to reconstruct the microbialites as the product of photic biomats that featured abundant cyanobacteria, while below this photic zone in a few millimeter depth, sulphate reducing and other heterotrophic microbes are suspected to drive larger scale mineralization, producing peloidal textures typical for microbialites, as evidenced by pyrite framboids (Fig. 5). They seem to drive oversaturation of the porewater with respect to HMC as evidenced in the peloidal texture, and with aragonite in deeper layers of the microbialite where it precipitates as syntaxial needle cement. While this model seems conclusive for the humid, windward side of the island, it is less evidenced on the dry side where the bioindicators of cyanobacteria have not been found. The question remains open as to why the record recovered on the humid side of the Island of Hawai'i contains such well-preserved cyanobacterial traces compared to the arid side, as well as to the substantially younger, last deglacial, successions

https://doi.org/10.5194/egusphere-2026-1564
Preprint. Discussion started: 9 April 2026

recovered in Tahiti (IODP 310) and the glacial maximum to deglacial aged ones from the GBR (IODP 325) (Westphal et al., 2010; Braga et al. 2019). The microbialites lacking cyanobacterial remains could represent cryptic, aphotic setting where cyanobacteria did not thrive. Figure 9 schematically illustrates the different environments in a coral reef where microbialites may form under varying photic conditions. While aphotic microbialites are known from modern reef cavities and are typically characterized by abundant sponge or ascidian spicules (Reitner, 1993; Gischler et al., 2017; Maak et al., 2024), in the present study, on the humid side of Hawaii, ascidians cooccur with cyanobacteria, pointing to shaded settings between platy corals in the euphotic zone. For the arid side of Hawaii, either an aphotic cryptic origin of the microbialites or poor preservation of the surface mat could explain the absence of preserved biomorphs. This study emphasizes the point that reefal microbialites represent a diverse set of precipitates that may have different origins in different environmental settings within the reef. Understanding their differences and similarities should render them more useful as environmental archives.

Author contributions

JMW acted as co-chief scientist of expedition IODP 389 and was thus instrumental in designing and conducting the cruise and securing the core material; HW designed the present study; HW and MG prepared the sample material; HW, EGa, and MG conducted the SEM and EDX analyses; HW, EGa and GEW interpreted the data with contributions by all authors; AM did the artwork in Figures 5 and 9; HW drafted the first version of the manuscript; all co-authors substantially contributed to the manuscript.

Competing interests

The authors declare no conflicts of interest.

Acknowledgements

We are grateful to Sebastian Flotow for support with the preparation of the samples and operation of the SEM at ZMT. Maximilian Göbel (Bremen University) helped with preparation of the samples and the SEM work at ZMT. This work is part of the research to fulfill the obligations of the IODP X389 Science party of which HW, PK, TN, EGi, and JMW are members. We are indebted to the IODP, Bremen Core Repository (MARUM, University of Bremen), and British Geological Service personnel supporting the work on IODP X389.

Financial support

This research was funded by ZMT baseline funding to HW. JMW and GEW acknowledge support provided by the Australian Research Council (Grant No. DP250102180) and ANZIC (Grant No. PCAFX38901).

https://doi.org/10.5194/egusphere-2026-1564
Preprint. Discussion started: 9 April 2026

References

Allwood, A.C., Walter, M.R., Kamber, B.S., Marshall, C.P., Burch, I.W. (2006) Stromatolite reef from the Early Archaean era of Australia. Nature, 441(7094), 714–718.

Andres, M.S., Reid, R.P. (2006) Growth morphologies of modern marine stromatolites: a case study from Highborne Cay, Bahamas. Sedimentary Geology, 185(3–4), 319–328.

Baud, A., Cirilli, S., Marcoux, J. (1997) Biotic response to mass extinction: the lowermost Triassic microbialites. Facies, 36, 238-242.

Berger A, Loutre MF (1991) Insolation values for the climate of the last 10 million years. Quaternary Science Reviews, 10(4):297–317. https://doi.org/10.1016/0277-3791(91)90033-Q

Braga JC, Puga-Bernabéu Á, Heindel K, Patterson MA, Birgel D, Peckmann J, Sánchez-Almazo IM, Webster JM, Yokoyama Y, Riding R (2019) Microbialites in Last Glacial Maximum and deglacial reefs of the Great Barrier Reef (IODP Expedition 325, NE Australia): Palaeogeography, Palaeoclimatology, Palaeoecology, v. 514, 1-17.

Burne, R. V., Moore, L. S. (1987) Microbialites: Organosedimentary deposits of benthic microbial communities. Palaios, 2(3), 241–254.

Camoin GF, Montaggioni L (1994) High energy coralgal-stromatolite frameworks from Holocene reefs (Tahiti, French Polynesia). Sedimentology, 41: 655–676.

Camoin GF, Gautret P, Montaggioni L, Cabioch G (1999) Nature and environmental significance of microbialites in Quaternary reefs: the Tahiti paradox. Sedimentary Geology, 126: 271-304.

de Bakker, D. M., Perry, C. T., Magana-Gallegos, E., Perez-Cervantes, E., Alvarez-Filip, L. (2024) Fine-grained sediment production by endolithic sponges on Caribbean coral reefs. Limnology and Oceanography, 69(9), 2015–2028. https://doi.org/10.1002/lno.12640

Degen, T., Sadki, M., Bron, E., König, U., Nénert, G. 2014. The HighScore suite. Powder Diffraction, 29 (S2), S13-S18. doi:10.1017/S0885715614000840.

Dohnalkova, A. C., Marshall, M. J., Arey, B. W., Williams, K. H., Buck, E. C., Fredrickson, J. K. (2011) Imaging hydrated microbial extracellular polymers: comparative analysis by electron microscopy. Applied and environmental microbiology, 77(4), 1254-1262.

Dupraz C, Strasser A (2002) Nutritional modes in coral-microbialite reefs (Jurassic, Oxfordian, Switzerland): Evolution of trophic structure as a response to environmental change, Palaios, 2002, 17: 449-471.

https://doi.org/10.5194/egusphere-2026-1564
Preprint. Discussion started: 9 April 2026

Dupraz, C., Visscher, P.T. (2005) Microbial lithification in marine stromatolites and hypersaline mats. Trends in Microbiology, 13(9), 429–438.

Dupraz, C., Reid, R.P., Braissant, O., Decho, A.W., Norman, R.S., Visscher, P.T. (2009) Processes of carbonate precipitation in modern microbial mats. Earth-Science Reviews, 96(3–4), 141–162.

Eckhardt, S., Ainsworth, T. D., Leggat, W., Page, C. E. (2024). Colonial ascidian populations at inshore coral reefs of Norfolk Island, South Pacific. Diversity, 16(7), 384, https://doi.org/10.3390/d16070384

Expedition 310 Scientists (2007) Expedition 310 summary. In: Camoin GF, Iryu Y, McInroy DB, and the Expedition 310 Scientists. Proc. IODP, 310: Washington, DC (Integrated Ocean Drilling Program Management International, Inc.). https://doi.org/10.2204/iodp.proc.310.101.2007

Falkenberg, P., Vahrenkamp, S., Garuglieri, E., Petrovic, A., Hachmann, K., Chandra, V., Vahrenkamp, V. (2026) Polygonal tepee structures of Arabia. The Depositional Record, 12, e70043. https://doi.org/10.1002/dep2.70043

Garuglieri, E., Marasco, R., Odobel, C., Chandra, V., Teillet, T., Areias, C., ... & Daffonchio, D. (2024). Searching for microbial contribution to micritization of shallow marine sediments. Environmental microbiology, 26(2), e16573.

Gischler, E., Heindel, K., Birgel, D., Brunner, B., Reitner, J., Peckmann, J. (2017). Cryptic biostalactites in a submerged karst cave of the Belize Barrier Reef revisited: pendant bioconstructions cemented by microbial micrite. Palaeogeography Palaeoecology Palaeoclimatology, 468, 34-51.

Gomes, M. L., Klatt, J. M., Dick, G. J., Grim, S. L., Rico, K. I., Medina, M., Ziebis, W., Kinsman-Costello, L., Sheldon, N. D., Fike, D. A. (2022). Sedimentary pyrite sulfur isotope compositions preserve signatures of the surface microbial mat environment in sediments underlying low-oxygen cyanobacterial mats. Geobiology, 20, 60–78. https://doi.org/10.1111/gbi.12466

Grotzinger, J. P., Knoll, A. H. (1999) Stromatolites in Precambrian carbonates: Evolutionary mileposts or environmental dipsticks? Annual Review of Earth and Planetary Sciences, 27, 313–358.

Hardy, R.G., Tucker, M. (1988) X-ray powder diffraction of sediments. In: Tucker, M. (ed.): Techniques in sedimentology. 191–228, Oxford Blackwell

Heindel K, Birgel D, Brunner B, Thiel V, Westphal H, Gischler E, Ziegenbalg SB, Cabioch G, Sjövall P, Peckmann J (2012) Post-glacial microbialite formation in coral reefs in the Pacific, Atlantic, and Indian Ocean. Chemical Geology 304-305, 117–130. https://doi.org/10.1016/j.chemgeo.2012.02.009

Heindel K, Birgel D, Peckmann J, Kuhnert H, Westphal H (2009a) Sulfate-reducing bacteria as major players in the formation of reef-microbialites during the last sea-level rise (Tahiti, IODP 310). Geochimica et Cosmochimica Acta, 73 (13), Goldschmidt Conference A514-A514

Heindel K, Birgel D, Peckmann J, Kuhnert H, Westphal H (2010) Formation of deglacial microbialites in coral reefs off Tahiti (IODP 310) involving sulfate-reducing bacteria. Palaios 25, 618–635. https://doi.org/10.2110/palo.2010.p10-032r

https://doi.org/10.5194/egusphere-2026-1564
Preprint. Discussion started: 9 April 2026

Heindel K, Westphal H, Wisshak M (2009b) Bioerosion in the reef framework, IODP Expedition #310 off Tahiti (Tiarei, Mara'a, and Faa'a); In Camoin GF, Iryu Y, McInroy DB, and the Expedition 310 Scientists, Proceedings IODP, 310, 28 p. https://doi.org/10.2204/iodp.proc.310.201.2009

Heindel K, Wisshak M, Westphal H (2009c) Microbioerosion in Tahitian reefs: a record of environmental change during the last deglacial sea-level rise (IODP #310). Lethaia 42, 322-340. https://doi.org/10.1111/j.1502-3931.2008.00140.x

Holtedahl, O. (1919) The Paleozoic formations of Finmarken in northern Norway. American Journal of Science, 4(278), 85-107.

Imbrie, J., Hays, J.D., Martinson, D.G., McIntyre, A., Mix, A.C., Morley, J.J., Pisias, N.G., Prell, W.L., Shackleton, N.J. (1984) The orbital theory of Pleistocene climate: support from a revised chronology of the marine δ18O record. Proceedings of the NATO Advanced Research Workshop, 1984:269. https://ui.adsabs.harvard.edu/abs/1984mcur.conf.269I

Jell, J.S., Webb, G.E. (2012) Geology of heron island and adjacent reefs, Great Barrier Reef, Australia. Episodes 35 (1), 110–119.

Kahal, A.Y., El-Sorogy, A., Alfaifi, H., Almadani, S., Kassem, O. (2019) Biofacies and diagenetic alterations of the Pleistocene coral reefs, northwest Red Sea coast, Saudi Arabia. Geological Journal, 55, 1380–1390.

Kurtz, A.C., Derry, A.D., Chadwick, O.A. (2001) Accretion of Asian dust to Hawaiian soils: isotopic, elemental, and mineral mass balances, Geochimica et Cosmochimica Acta, 65, 1971-1983, https://doi.org/10.1016/S0016-7037(01)00575-0.

Lambeck K, Chappell J (2001) Sea level change through the last glacial cycle. Science, 292(5517):679–686. https://doi.org/10.1126/science.1059549

Lea DW, Martin PA, Pak DK, Spero HJ (2002) Reconstructing a 350 ky history of sea level using planktonic Mg/Ca and oxygen isotope records from a Cocos Ridge core. Quaternary Science Reviews, 21(1):283–293. https://doi.org/10.1016/S0277-3791(01)00081-6

Lin, F., Zhu, X., Li, J., Yu, P., Luo, Y., Liu, M. (2019) Effect of extracellular polymeric substances (EPS) conditioned by combined lysozyme and cationic polyacrylamide on the dewatering performance of activated sludge. Chemosphere, 235, 679-689.

Ludwig KR, Szabo BJ, Moore JG, Simmons KR (1991) Crustal subsidence rate off Hawaii determined from 234U/238U ages of drowned coral reefs. Geology, 19(2):171–174. https://doi.org/10.1130/0091-7613(1991)019<0171:CSROHD>2.3.CO;2

Maak, J.M., Birgel, D., Reitner, J., Gischler, E., Dullo, W.C., Foster, W., Peckmann, J. (2024). Molecular fossils in microbial carbonates and sponges of the deep fore reef of Mayotte and Moheli, Comoro Islands. Facies, 70, doi.org/10.1007/s10347-023-00678-3

Marshall JF, Davies PJ (1988) Halimeda bioherms of the northern Great Barrier Reef. Coral Reefs, 6: 139–148.

Melim LA, Northup DE, Spilde MN, Boston PJ (2015) Update: Living reticulated filaments from Herbstlabyrinth-Adventhöhle Cave System Germany. Journal of Cave and Karst Studies 77(2), 87–90. DOI: 10.4311/2015MB0112

https://doi.org/10.5194/egusphere-2026-1564
Preprint. Discussion started: 9 April 2026

Nothdurft LD, Webb GE, Bostrom T, Rintoul L (2007) Calcite-filled borings in the most recently deposited skeleton in live-collected Porites (Scleractinia): implications for trace element archives. Geochimica et Cosmochimica Acta 71:5423–5438. doi:10.1016/j.gca.2007.09.025

Pei Y, Hagdorn H, Voigt T, Duda J-P, Reitner J (2022) Palaeoecological Implications of Lower-Middle Triassic Stromatolites and Microbe-Metazoan Build-Ups in the Germanic Basin: Insights into the Aftermath of the Permian–Triassic Crisis. Geosciences 12(3), 133. https://doi.org/10.3390/geosciences12030133

Perri, E., Tucker, M.E., Słowakiewicz, M., Whitaker, F., Bowen, L., Perrotta, I.D. (2018) Carbonate and silicate biomineralization in a hypersaline microbial mat (Mesaieed sabkha, Qatar): Roles of bacteria, extracellular polymeric substances and viruses. Sedimentology, 65: 1213-1245. https://doi.org/10.1111/sed.12419

Power IM, Wilson SA, Thom JM, Dipple GM, Southam G (2007) Biologically induced mineralization of dypingite by cyanobacteria from an alkaline wetland near Atlin, British Columbia, Canada. Geochem Trans 8:13, doi:10.1186/1467-4866-8-13

Pratt, B.R. (1982) Stromatolite decline—a reconsideration: Geology, v. 10, p. 512–515.

Puga-Bernabéu, Á., Webster, J.M., Braga, J.C., Clague, D.A., Dutton, A., Eggins, S., Fallon, S., Jacobsen, G., Paduan, J.B., and Potts, D.C., 2016. Morphology and evolution of drowned carbonate terraces during the last two intergla-cial cycles, off Hilo, NE Hawaii. Marine Geology, 371:57–81. https://doi.org/10.1016/j.margeo.2015.10.016

Reid P, Visscher TP, Decho AW, Stolz JF, Bebout BM, Dupraz C, MacIntyre IG, Paerl HW, Pinckney JL, Prufert-Bebout L, Steppe TF, DesMarais DJ (2000) The role of microbes in accretion, lamination, and early lithification of modern marine stromatolites. Nature, 406: 989-992.

Reitner J (1993) Modern cryptic microbialite-metazoan facies from Lizard Island (Great Barrier Reef, Australia), formation and concepts. Facies, 29: 3–40.

Reitner J, Gautret P, Marin F, Neuweiler F (1995) Automicrites in a modern microbialite. Formation model via organic matrices (Lizard Island, Great Barrier Reef, Australia). Bull. Inst. Océanogr. Monaco, 14: 237-263.

Reitner, J., Thiel, V., Zankl, H., Michaelis, W., Wörheide, G., Gautret, P. (2000) Organic and biogeochemical patterns in cryptic microbialites. In Microbial sediments (pp. 149-160). Berlin, Heidelberg: Springer Berlin Heidelberg.

Ribes M., Coma R., Atkinson M.J., Kinzie R.A.III (2005) Sponges and ascidians control removal of particulate organic nitrogen from coral reef water, Limnol. Oceanogr., 50(5), 2005, 1480–1489

Riding, R. (2000a) Microbial carbonate abundance compared with fluctuations in metazoan diversity over geological time. Sedimentary Geology, 134(1–2), 13–26.

Riding R (2000b) Microbial carbonates: the geological record of calcified bacterial-algal mats and biofilms. Sedimentology, 47: 179-214.

Riding, R. (2006) Microbial carbonate abundance compared with fluctuations in metazoan diversity over geological time. Sedimentary Geology, 185(3–4), 229–238.

https://doi.org/10.5194/egusphere-2026-1564
Preprint. Discussion started: 9 April 2026

Riding, R. (2011) Microbialites, stromatolites, and thrombolites. In Reefs in Time and Space: The History and Evolution of the Reef-Building Biota (pp. 103–120).

Riding, R. and Awramik, S.M. (Eds.) (2000) Microbial Sediments. Springer Verlag, Heidelberg, 331 p.

Riding, R., Liang, L., Braga, J.C. (2014) Millennial-scale ocean acidification and late Quaternary decline of cryptic bacterial crusts in tropical reefs. Geobiol., 12, 387-405.

Riker-Coleman K, Gallup C, Clague D, Webster JM, Edwards L, Cheng H (2005) New 230Th ages from the – 400 m reef of northwestern Hawaii. Eos, Transactions of the American Geophysical Union, 86(52): PP21C-1574. https://abstractsearch.agu.org/meetings/2005/FM/PP21C-1574.html

Robles-Fernández, A., Areias, C., Daffonchio, D., Vahrenkamp, V. C., Sánchez-Román, M. (2022). The Role of Microorganisms in the Nucleation of Carbonates, Environmental Implications and Applications. Minerals, 12(12), 1562. https://doi.org/10.3390/min12121562

Salas-Saavedra, M., Dechnik, B., Webb, G.E., Webster, J.M., Zhao, J.-X., Nothdurft, L.D., Clark, T.R., Graham, T., Duce, S. (2018) Holocene reef growth over irregular Pleistocene karst confirms major influence of hydrodynamic factors on Holocene reef development. Quaternary Science Reviews, 180, 157–176. https://doi.org/10.1016/j.chemgeo.2022.120871

Sanborn KL, Webster JM, Yokoyama Y, Dutton A, Braga JC, Clague DA, Paduan JB, Wagner D, Rooney JJ, and Hansen JR (2017) New evidence of Hawaiian coral reef drowning in response to meltwater pulse-1A. Quater-nary Science Reviews, 175:60–72. https://doi.org/10.1016/j.quascirev.2017.08.022

Sanfilippo, K., Timm, O. E., Frazier, A. G., Giambelluca, T. W. (2024) Effects of systematic predictor selection for statistical downscaling of rainfall in Hawai'i. International Journal of Climatology, 44(2), 571–591. https://doi.org/10.1002/joc.8345

Schubert, J.K., Bottjer, D.J. (1992) Early Triassic stromatolites as post-mass extinction disaster forms: Geology, v. 20, p. 883–886.

Séard C, Camoin G, Yokoyama Y, Matsuzaki H, Durand N, Bard E, Sepulcre S, Deschamps P (2011) Microbialite development patterns in the last deglacial reefs from Tahiti (French Polynesia; IODP Expedition #310): Implications on reef framework architecture. Marine Geology, 279, 63-86, https://doi.org/10.1016/j.margeo.2010.10.013.

Shirokova, L.S., Mavromatis, V., Bundeleva, I.A. et al. (2013) Using Mg Isotopes to Trace Cyanobacterially Mediated Magnesium Carbonate Precipitation in Alkaline Lakes. Aquat Geochem 19, 1–24. https://doi.org/10.1007/s10498-012-9174-3

Stolz, J, Reid, R.P., Visscher, P., Decho, A., Norman, R., Aspden, R., Bowlin, E., Franks, J., Foster, J., Paterson, D., Przekop, K., Underwood, G. Prufert-Bebout, L. (2009). The Microbial Communities of the Modern Marine Stromatolites at Highborne Cay, Bahamas. Atoll Research Bulletin. 567. 10.5479/si.00775630.567.1.

Swart, P.K., Melim, L.A. (2000) The origin of dolomites in Tertiary sediments from the margin of Great Bahama Bank. Journal of Sedimentary Research, 70, 738–748.

https://doi.org/10.5194/egusphere-2026-1564
Preprint. Discussion started: 9 April 2026

Szilagyi Z, Webster JM, Patterson MA, Hips K, Riding R, Foley M, Humblet M, Yokoyama Y, Liang L, Gischler E, Montaggioni L, Gherardi D, Braga JC (2020) Controls on the spatio-temporal distribution of microbialite crusts on the Great Barrier Reef over the past 30,000 years: Marine Geology. https://doi.org/10.1016/j.margeo.2020.106312

595 Taylor B (2019) Shoreline slope breaks revise understanding of Hawaiian shield volcanoes evolution. Geochemistry, Geophysics, Geosystems, 20(8):4025–4045. https://doi.org/10.1029/2019GC008436

van Lith, Y., Warthmann, R., Vasconselos, C., McKenzie, J.A. (2003). Sulphate-reducing bacteria induce low-temperature Ca-dolomite and high Mg-calcite formation. Geobiology, 1, 71–79.

Visscher, P.T., Stolz, J.F. (2005). Microbial mats as bioreactors: populations, processes, and products. Palaeogeography,
600 Palaeoclimatology, Palaeoecology, 219(1–2), 87–100.

Vogt, C., Lauterjung, J., Fischer, R.X., 2002. Investigation of the clay fraction (<2 µm) of the clay mineral society reference clays. Clays and Clay Minerals, 50(3): 388-400.

Watts AB (1978) An analysis of isostasy in the world's oceans, 1. Hawaiian-Emperor Seamount Chain. Journal of Geophysical Research: Solid Earth, 83(B12):5989–6004. https://doi.org/10.1029/JB083iB12p05989

605 Webb, G.E. (1996) Was Phanerozoic reef history controlled by the distribution of nonenzymatically secreted reef carbonates (microbial carbonate and biologically induced cement)? Sedimentology, v. 43, p. 947–971.

Webb, G.E., (2005) Quantitative Analysis and Paleoecology of Earliest Mississippian Microbial Reefs, Gudman Formation, Queensland, Australia: Not Just Post-Disaster Phenomena. Journal of Sedimentary Research. 75. 875-894. 10.2110/jsr.2005.068.

610 Webb, G.E., Kamber, B.S. (2000) Rare earth elements in Holocene reefal microbialites: a new shallow seawater proxy. Geochimica et Cosmochimica Acta 2000 Vol. 64 Issue 9 Pages 1557-1565. http://dx.doi.org/10.1016/S0016-7037(99)00400-7

Webster JM, Clague DA, Riker-Coleman K, Gallup C, Braga JC, Potts D, Moore JG, Winterer EL, Paull CK (2004) Drowning of the -150m reef off Hawaii: a casualty of global meltwater pulse 1A? Geology, 32(3):249– 252.
615 https://doi.org/10.1130/G20170.1

Webster JM, Wallace LM, Clague DA, Braga JC (2007) Numerical modeling of the growth and drowning of Hawaiian coral reefs during the last two glacial cycles (0–250 kyr). Geochemistry, Geophysics, Geosystems, 8(3):Q03011. https://doi.org/10.1029/2006GC001415

Webster JM, Braga JC, Clague DA, Gallup C, Hein JR, Potts DC, Renema W, Riding R, Riker-Coleman K, Silver E, Wallace
620 LM (2009) Coral reef evolution on rapidly subsiding margins. Global and Planetary Change, 66(1–2):129–148. https://doi.org/10.1016/j.gloplacha.2008.07.010

Webster JM, Ravelo AC, Grant HLJ (2023) Expedition 389 Scientific Prospectus: Hawaiian Drowned Reefs. International Ocean Discovery Program. https://doi.org/10.14379/iodp.sp.389.2023

Webster, J.M., Ravelo, A.C., Grant, H.L.J., and the Expedition 389 Scientists, 2024. Expedition 389 Preliminary Report:
625 Hawaiian Drowned Reefs. International Ocean Discovery Program. https://doi.org/10.14379/iodp.pr.389.2024

https://doi.org/10.5194/egusphere-2026-1564
Preprint. Discussion started: 9 April 2026

Webster, J.M., Ravelo, A.C., Grant, H.L.J., and the Expedition 389 Scientists, 2025. Hawaiian Drowned Reefs. Proceedings of the International Ocean Discovery Program, 389: College Station, TX (International Ocean Discovery Program). https://doi.org/10.14379/iodp.proc.389.2025

Westphal H, Heindel K, Brandano M, Peckmann J (2010) Genesis of microbialites as contemporaneous framework components of coral reefs, deglacial of Tahiti (IODP 310). Facies 56, 337-352. https://doi.org/10.1007/s10347-009-0207-3

White, B., Kurkjy, K.A., Curran, H.A., Besom, K.A. (1984) Shallowing-upward sequence in a Pleistocene coral reef and associated facies, San Salvador, Bahamas. AAPG Bulletin, 68, 539–539.

Zhang, H.S.; Dai, M.-Y.; Qi, Y.-A.; Han, L.-L.; Yin, Z.-L.; Chen, S.-H.; Lin, L.-B. (2024) Girvanella fossils from the Phanerozoic: Distribution, evolution and controlling factors. J. Palaeogeogr., 13, 924–938.

https://doi.org/10.5194/egusphere-2026-1564
Preprint. Discussion started: 9 April 2026

Appendix A: Line scans of H2-terrace reef cores studied here by means of SEM. Core width is 7.2 cm.

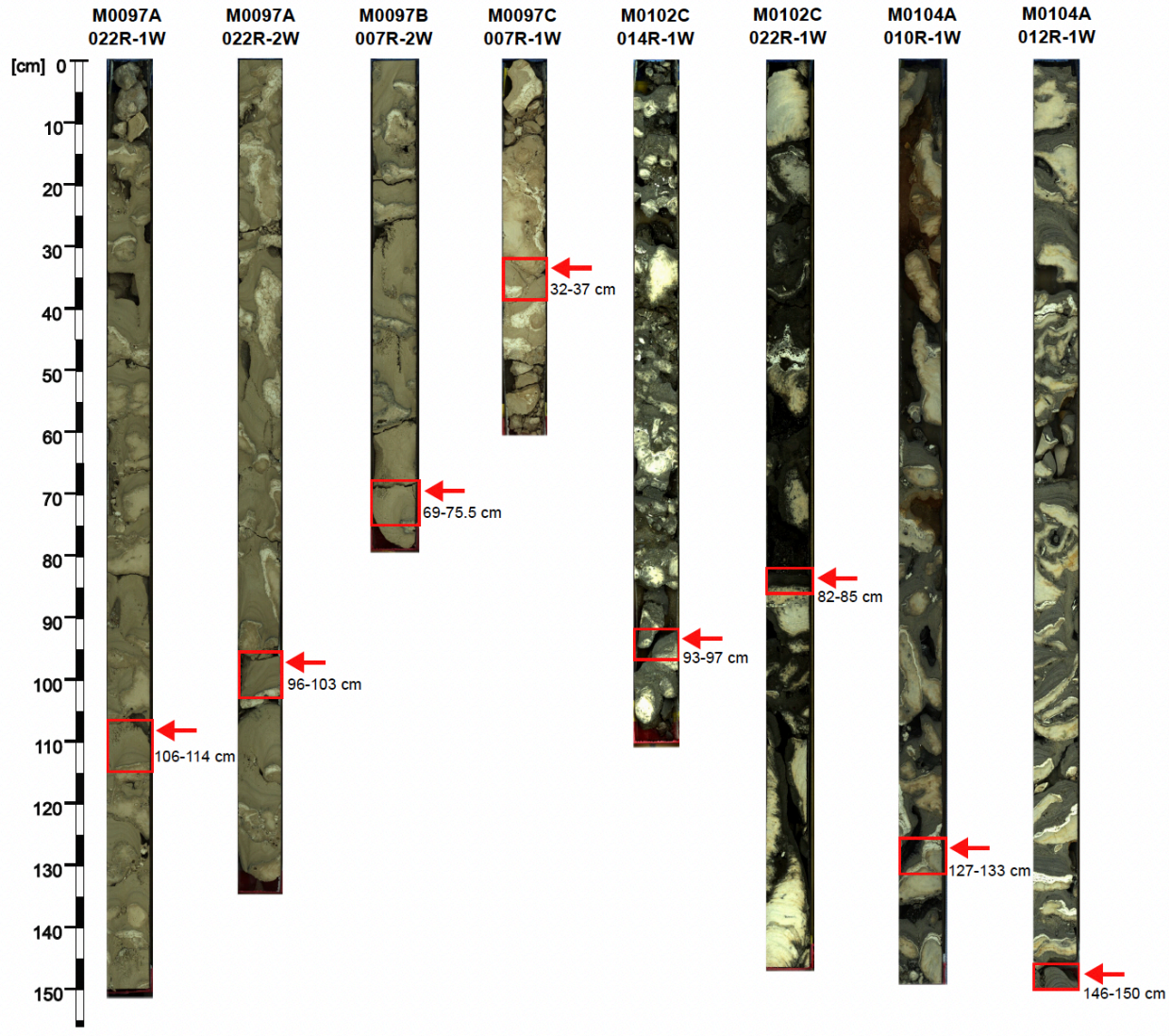

640

https://doi.org/10.5194/egusphere-2026-1564
Preprint. Discussion started: 9 April 2026

Appendix B: Samples from IODP Expedition 389 studied here.

Side of Island	Site	Sample ID	Estimated age range (Webster et. al. 2025)	SEM	XRD
Windward, humid	Kohala	M0102_C_014R_1W 93 - 97 cm	171-225 ky	X	X
Windward, humid	Kohala	M0102_C_022R_1W 82-85 cm	171-225 ky	X	X
Windward, humid	Hilo	M0104_A_010R_1W 127-133 cm	130-159 ky	X	X
Windward, humid	Hilo	M0104_A_012R_1W 146-150 cm	130-159 ky	X	X
Windward, humid	Hilo	M0104_A_013R_11W_11-20 cm	130-159 ky		X
Leeward, arid	Kawaihae	M0097_A_022R_1W 106 -114 cm	133-150 ky	X	X
Leeward, arid	Kawaihae	M0097_A_022R_2W 96-103 cm	133-150 ky	X	X
Leeward, arid	Kawaihae	M0097_B_007R_2W 69-75.5 cm	133-150 ky	X	X
Leeward	Kawaihae	M0097_B_007A_2W_93-76.5 cm	133-150 ky		X
Leeward	Kawaihae	M0097_C_007R_1W 32-37 cm	133-150 ky	X	X

https://doi.org/10.5194/egusphere-2026-1564
Preprint. Discussion started: 9 April 2026

Appendix C: EDX spectra of entrapped non-carbonate grains; sample M0104A-012R-1, 146-150 cm.

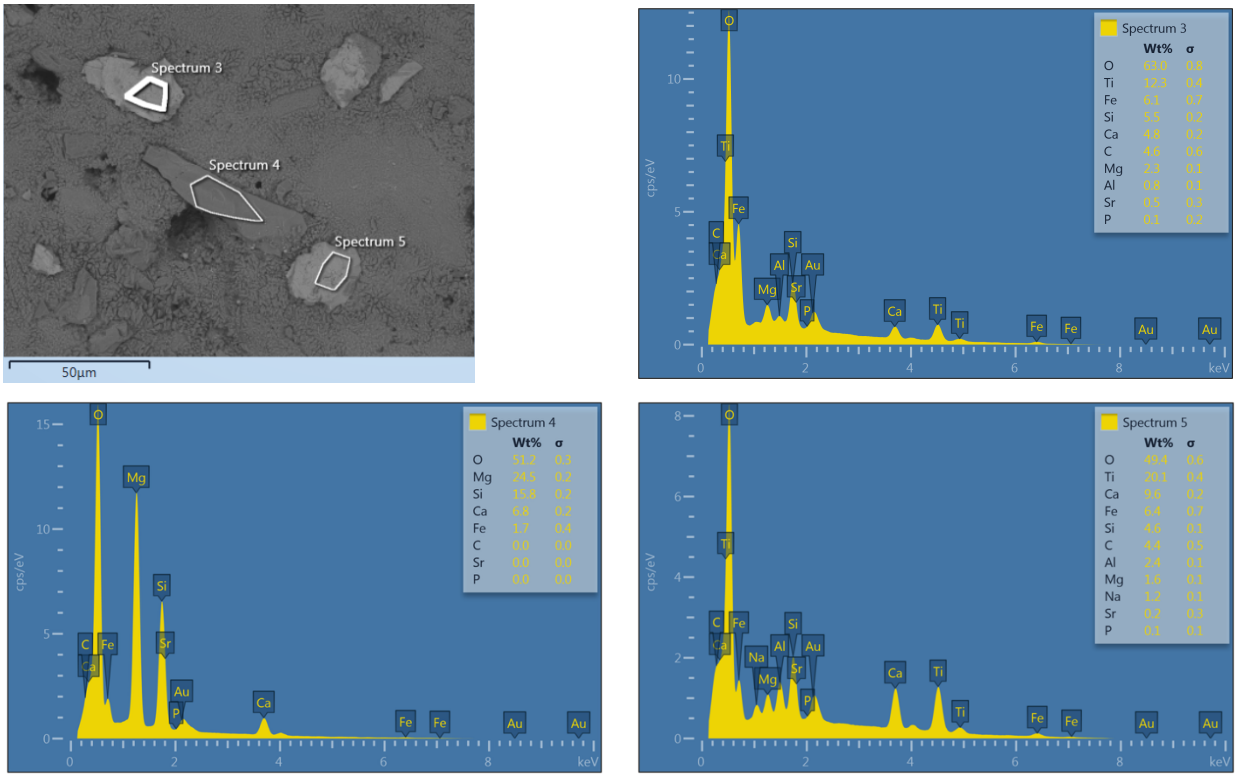

645

https://doi.org/10.5194/egusphere-2026-1564
Preprint. Discussion started: 9 April 2026

Appendix D: EDX spectra of flaky minerals, sample M0104A-012R-1, 146-150 cm.

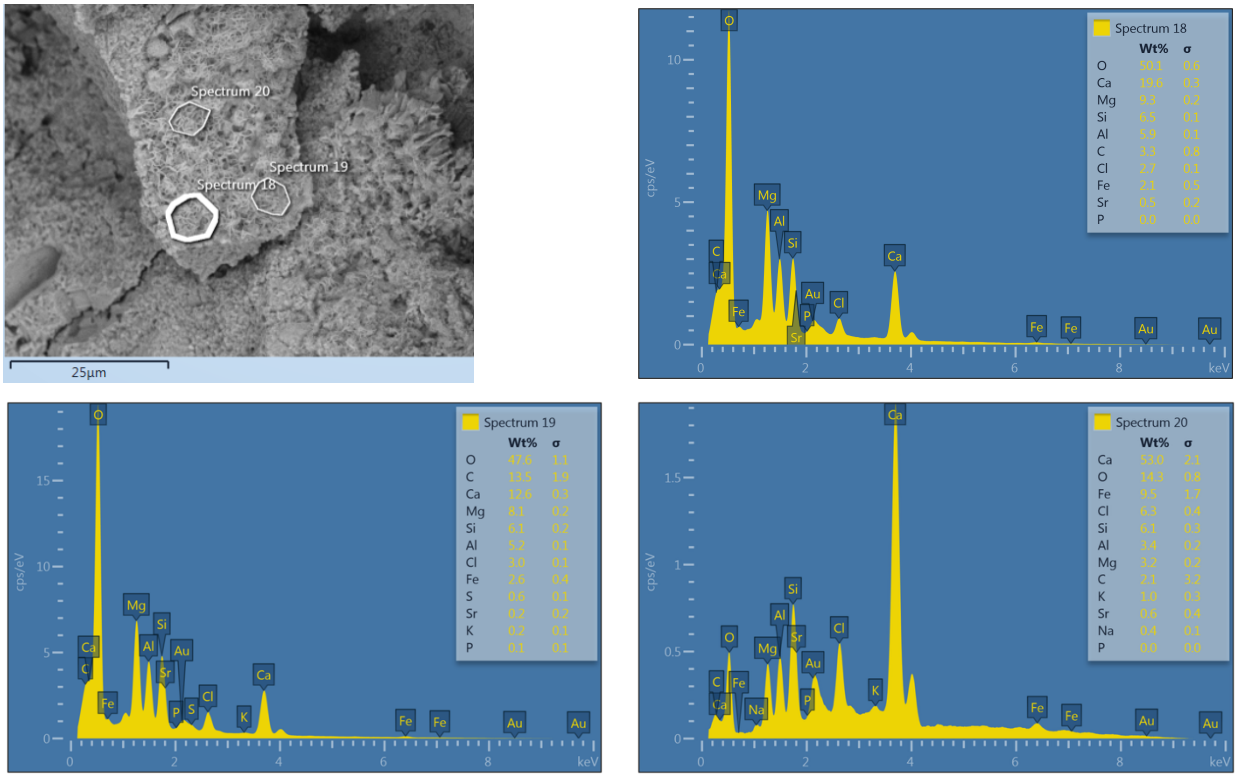

650

https://doi.org/10.5194/egusphere-2026-1564
Preprint. Discussion started: 9 April 2026

Appendix E: Mineralogical composition according to XRD results in %. HMC indicates high-Magnesium calcite.

Side of Island	sample	HMC	Aragonite	Anorthite	others
Windward	M102C_014R_1W 93-97	62	31	4	3 (Muscovite, Brushite)
Windward	M102C-022R-1W_82-85	79	9	7	4 (Richterite, Gypsum)
Windward	M104A-010R-21W_124-133	81	13	3	3 (Quartz)
Windward	M104A-012R_1W_146-150	78	15	0	7 (Quartz, Ilmenite, Ramsdellite)
Windward	M104A-013R-11W_11-20	80	13	7	0
Leeward	M097A-022R_1W_106-114	87	12	0	1 (Huntite)
Leeward	M097A_022R_2W_96-103	88	12	0	0
Leeward	M097B-007A-2W_93-76.5	89	9	0	2 (Huntite, Pyrolusite)
Leeward	M097B_007R_2W_69-75.5	81	13	0	6 (Calcite)
Leeward	M097C_007R_1W_32-37	81	19	0	0